



Influence of regional climate and local hydrological conditions on carbon accumulation process within the Jinchuan peatland (Northeast China) since the middle Holocene

Yanmin Dong ^{a,b,*}, Jing Li ^a, Sizhu Li ^a, Lu Yu ^a, Zhiwei Xu ^{a,b}, Shengzhong Wang ^{a,b}

^a Key Laboratory of Geographical Process and Ecological Security in Changbai Mountains, Ministry of Education, School of Geographical Sciences, Northeast Normal University, Changchun, 130024, China

^b State Environmental Protection Key Laboratory of Wetland Ecology and Vegetation Restoration, Institute for Peat and Mire Research, Northeast Normal University, Changchun, 130024, China

ARTICLE INFO

Handling Editor: Dr Yan Zhao

Keywords:

Peatland
Carbon accumulation rate
Climate
Local condition
Northeast China

ABSTRACT

Peatlands represent a vital component of the terrestrial carbon pool owing to their high carbon sequestration efficiency. A comprehensive understanding of the carbon accumulation process and its driving factors is essential to assess future carbon reservoir functions. Within a single peatland, carbon accumulation may differ among sites because of local conditions. However, this spatial variability has received little attention. To address this gap, four peat cores from the Jinchuan (JC) peatland in the Changbai Mountains were analyzed to investigate the spatial heterogeneity and consistency of carbon accumulation since the middle Holocene. ¹⁴C Accelerator Mass Spectrometry was used to establish the chronological framework of each core, and the organic carbon content and bulk density were measured to calculate the carbon accumulation rate (CAR). The moisture conditions at each sampling location were reconstructed using the carbon stable isotopes ($\delta^{13}\text{C}$) values of α -cellulose in *Carex* spp. residues. The influence of both regional climate and local hydrological conditions on CAR was analyzed. The results indicated that the CAR values for the four cores were 62.9, 53.4, 44.2, and 47.7 g C/m²/yr, respectively. The moisture conditions across the sampling sites generally declined over millennial timescales, which is consistent with the decreasing regional precipitation in the Changbai Mountains. Between 6.5 and 1.5 kyr BP, the spatial heterogeneity in CAR demonstrated that local factors, such as topography and moisture conditions, were the dominant controls. Over the last 1.5 kyr BP, the consistent CAR values across the JC peatland indicated that the regional climate became the primary driver. This study demonstrates that hydrological variation is the key factor driving spatial heterogeneity in CAR and highlights that the dominant controls on CAR may shift over time. These findings can improve our understanding of climate-driven carbon accumulation in peatlands by integrating local environmental influences.

1. Introduction

Peatlands can store approximately one-third of the world's terrestrial carbon and are among the most efficient terrestrial ecosystems for long-term carbon sequestration (Yu et al., 2011; Xu et al., 2018), playing a vital role in the global carbon cycle and in mitigating climate warming (Frolking and Roulet, 2007; Huang et al., 2021; Loisel et al., 2017). Exploring the carbon accumulation process in peatlands and its controlling factors is essential to elucidate the formation mechanisms of this significant carbon pool.

The initiation and development of peatlands over long temporal and spatial scales are closely linked to summer solar insolation, summer-winter climate seasonality, and regional precipitation and temperature (Jone and Yu, 2010; Zhao et al., 2014; Gallego-Sala et al., 2018), which influence carbon accumulation process by altering the balance between plant productivity and microbial decomposition (Charman, 2002; Rydin et al., 2006). For example, peatlands in Alaska exhibited higher carbon accumulation rates (CAR) during the early Holocene, a period marked by elevated summer temperatures and pronounced climate seasonality (Jone and Yu, 2010). Similar patterns, where warm and humid climates

* Corresponding author. Key Laboratory of Geographical Process and Ecological Security in Changbai Mountains, Ministry of Education, School of Geographical Sciences, Northeast Normal University, Changchun, 130024, China.

E-mail address: dongym809@nenu.edu.cn (Y. Dong).

promote an increased CAR, have also been observed in Siberia (Feurdean et al., 2019), Finland (Mathijssen et al., 2016), central-eastern Europe (Panait et al., 2017; Longman et al., 2021), North America (Charman et al., 2015; van Bellen et al., 2020; Perrier et al., 2022), and China (Zhao et al., 2014; Xing et al., 2015; Dong et al., 2021). Beyond climate, CAR is also influenced by local factors such as hydrological conditions, plant composition, and autogenic succession at the site scale (Loisel and Yu, 2013; Charman et al., 2015; Loisel et al., 2017; Piilo et al., 2020; Dong et al., 2021). For instance, CAR in southern Patagonian peatlands is more strongly governed by local vegetation and self-regulation mechanisms than by climate (Loisel and Yu, 2013), whereas in the Laolike peatland of the Changbai Mountains, a higher CAR is associated with wetter surface conditions (Dong et al., 2021). These findings highlight the multifactorial nature of carbon accumulation in peatlands and emphasize the need to consider both external climatic drivers and local internal processes.

Saturated soils and frequently waterlogged conditions are essential prerequisites for the initiation of peatlands (Charman, 2002). Moisture conditions are recognized as important environmental factors that regulate carbon accumulation in peatlands. However, the role of moisture in determining peatland CAR remains unclear (Charman et al., 2015; Liu et al., 2022; Perrier et al., 2022). Some studies have reported that wet conditions can enhance CAR (Mathijssen et al., 2019; Perrier et al., 2022), whereas others have indicated that the relationship between moisture and CAR is not consistently positive (Charman et al., 2015; Lacourse and Davies, 2015). For instance, among the three peatlands in northeastern North America, only one presents a weak but significant positive correlation between water table depth and CAR (Charman et al., 2015). In addition, recent research on the Dajiuju peatland in eastern central China and the Dongfanghong peatland in northeast China has revealed that CAR may exhibit a threshold response to hydrological conditions (Liu et al., 2022; Dong et al., 2024). These conflicting findings highlight the complex, potentially non-linear relationships between hydrological parameters and carbon accumulation. Therefore, further in-depth investigation is required to better elucidate this relationship.

Long-term carbon accumulation in peatlands can be assessed through analysis of peat cores extracted using various techniques (De Vleeschouwer et al., 2010). Typically, cores obtained from the depositional centers of peatlands or those with the longest temporal records are frequently utilized to reconstruct CAR and examine the associated influencing factors (e.g., Primeau and Garneau, 2021; Perrier et al., 2022; Dong et al., 2024). Previous studies have demonstrated spatial heterogeneity in hydrological conditions and plant composition within peatlands (Loisel and Garneau, 2010; Robitaille et al., 2021; Dong et al., 2021, 2023). For example, the water table depth at different locations within the Misask and Cheinu peatlands in north-central Quebec exhibited distinct variation patterns during the same period (Robitaille et al., 2021). Differences in plant composition were observed between the two peat cores located approximately 1.5 km apart in the Siikaneva peatland in southern Finland (Mathijssen et al., 2016). These spatial heterogeneities may lead to variations in carbon accumulation patterns across different locations within the same peatland (Loisel and Garneau, 2010; Mathijssen et al., 2019; Piilo et al., 2020; Dong et al., 2021). Despite the known influence of core location on CAR, current CAR reconstructions predominantly rely on single-core analyses, whereas multi-core integration remains limited (Piilo et al., 2020; Mathijssen et al., 2016; Dong et al., 2023). This methodological limitation increases the uncertainty of the reconstructed CAR values and ultimately constrains the predictive capabilities of the peatland carbon sink dynamics under climate change. Multi-core analysis facilitates differentiation between the effects of climatic factors and local conditions on carbon accumulation.

In this study, four cores from a minerotrophic fen in the Changbai Mountains of Northeast China were analyzed to reconstruct the CAR and moisture conditions since the middle Holocene. The influence of the

regional climate and local hydrological conditions on peatland carbon dynamics was investigated. This study aimed to (i) illustrate an example of spatial heterogeneity in carbon accumulation within a peatland, (ii) elucidate the differential responses of CAR to regional climate at various locations, and (iii) identify the role and underlying mechanisms of local hydrological conditions in the carbon accumulation process.

2. Study site

The Jinchuan (JC) peatland (42°20'48"N, 126°21'48"E, 618 m) is situated in the Longgang Mountain range on the western foothills of the Changbai Mountains in northeastern China (Fig. 1a and b). The long-term meteorological records from a nearby station indicate that the JC peatland experiences an average annual temperature of 3.3 °C and receives over 700 mm of precipitation annually, with precipitation predominantly occurring in summer, reflecting a typical mid-temperate monsoon climate characterized by synchronized rainy and warm seasons (Fig. 1c). The peatland is surrounded by mixed coniferous and broadleaf forests (Fig. 1d), dominated by *Larix olgensis*, *Abies fabri*, *Betula platyphylla*, *Quercus mongolica*, and *Tilia amurensis* (Stebich et al., 2015). The primary water sources are atmospheric precipitation and surface runoff from the surrounding mountains, with the Hou River flowing along the eastern and southern margins. The current surface vegetation is mainly herbaceous, comprising species such as *Carex schmidii*, *Carex teruiflora*, *Phragmites australis*, *Thelypteris palustris*, *Hypericum japonicum*, and *Saussurea japonica*, while shrubs including *Lonicera caerulea*, *Spiraea salicifolia*, and *Betula fruticosa* are distributed along the northern and western edges. Based on the basal age distributions of peat deposits, the JC peatland was initiated approximately 7 kyr BP following the desiccation of a lake and subsequently expanded laterally through terrestrial paludification processes (Zhang et al., 2019).

3. Material and methods

3.1. Field investigation and sample collection

The aerial imagery and surface elevation data of the JC peatland were obtained using a DJI Mavic 2 Pro unmanned aerial vehicle equipped with a laser radar. A manual Russian-type peat corer was used at 95 sampling points to determine the peat thickness. Four continuous peat cores were extracted along a northeast-to-southwest transect and designated sequentially as JCPC-1 to JCPC-4 (Fig. 1d). After documenting the sedimentary characteristics and photographing the cores, each was sectioned *in situ* at 1 cm intervals (Fig. 2 and Table S1). Subsamples were transported to the laboratory and stored at 4 °C until further analysis. Although JCPC-3 and JCPC-4 contain composite sequences of lacustrine mud and peat (Fig. S1 and S2), this study focused exclusively on the analysis of the upper peat layers (Table S1).

3.2. Dating method

Chronological determination of the four cores was conducted using the Accelerator Mass Spectrometry radiocarbon dating method (AMS ^{14}C). The dating layers were selected based on sedimentary features such as peat color, degree of decomposition, and plant composition. The sampling intervals were approximately 30 cm for JCPC-1, JCPC-3, and JCPC-4 and 50 cm for JCPC-2. The materials used for AMS ^{14}C dating included aboveground herbaceous plant remains (e.g., stems, leaves, and seeds), *Sphagnum* moss, and bulk peat from highly decomposed layers (Table 1). All samples were subjected to acid-alkali-acid pretreatment (Olsson, 1986) and converted into graphite targets using a vacuum system at Northeast Normal University. Radiocarbon dating was performed using a 1.0 MV Tandetron Model 4110 BO accelerator mass spectrometer at the Taiwan University. The resulting ^{14}C ages were calibrated to calendar years using OxCal 4.4 online calibration tool with

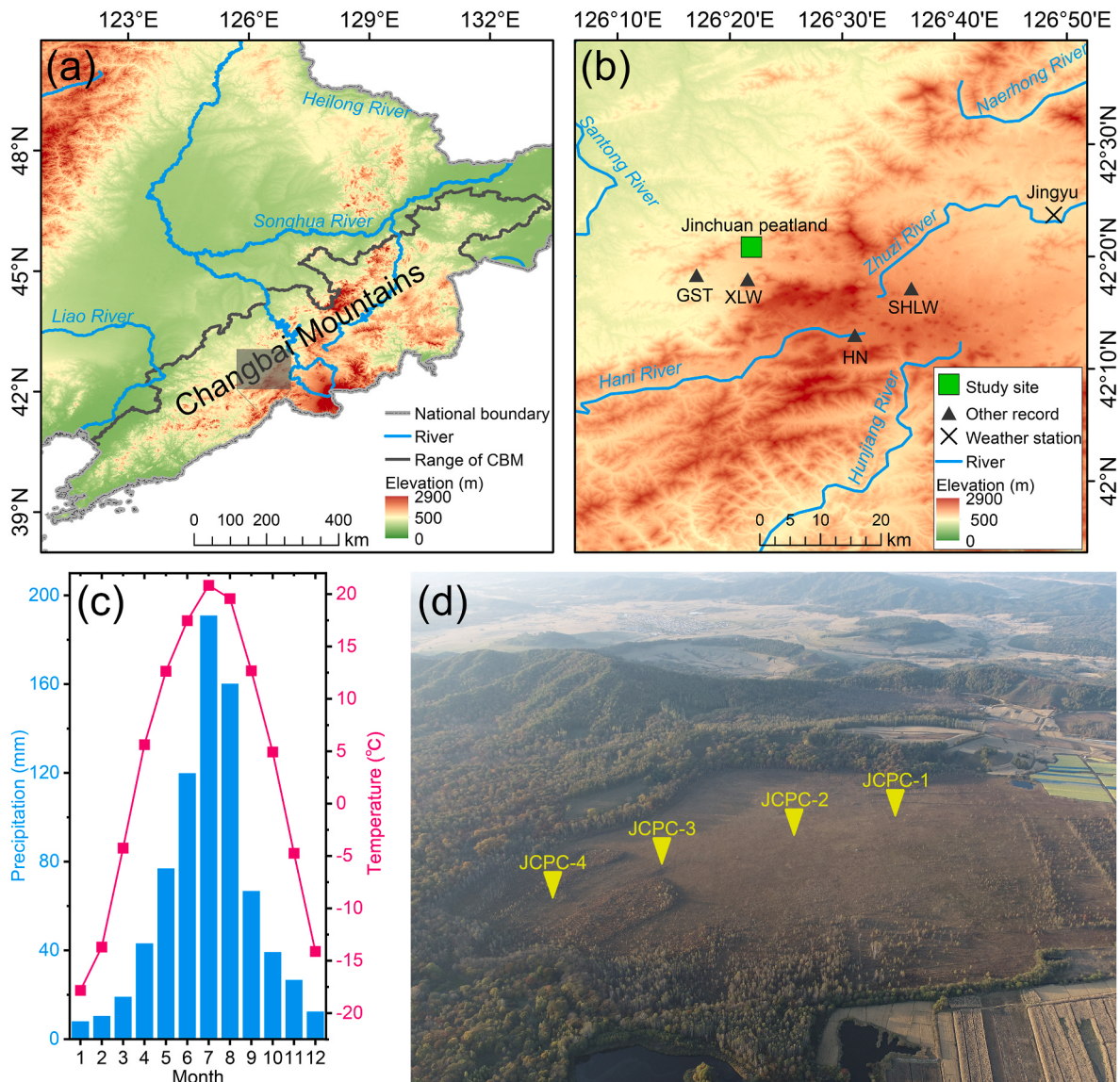


Fig. 1. (a) Geographical location of the Changbai Mountains (CBM). The black-shaded area represents the Longgang Mountain range, where the Jinchuan peatland is located. (b) Map showing the specific location of the Jinchuan (JC) peatland and nearby paleoclimate records, including those from the Sihailongwan Maar Lake (SHLW) (Stebich et al., 2015), the Gushantun (GST) peatland (Leng, 2019), the Xiaolongwan Maar Lake (XLW) (Xu et al., 2019), and the Hani (HN) peatland (Zheng et al., 2017). (c) Average monthly precipitation and temperature in the JC peatland recorded by the Jingyu meteorological station from 1980 to 2020. (d) Panoramic view of the JC peatland and locations of study core.

an IntCal20 calibration curve (Bronk, 2009; Reimer et al., 2020). The age-depth models for each core were developed using the Bacon package in R (Blaauw and Christen, 2011; Blaauw et al., 2019). All ages have been reported in kiloyears before the present (kyr BP), where 1 kyr BP = 1000 yr BP, with "BP" defined as years before 1950 CE.

3.3. Reconstruction of paleotopography

Using photographs with elevation data collected from the JC peatland, image synthesis was conducted using Agisoft Metashape Professional software to perform photogrammetric and elevation modeling (Fig. 3a and b). The surface elevation at the peat thickness survey points was then extracted, and the peat basal elevation was calculated by subtracting the peat thickness from the surface elevation. Spatial interpolation of the basal elevation data was performed in ArcMap 10.8 using the Kriging method. Based on the basal elevations and accumulation rates of the four examined cores, the surface elevation evolution of the JC peatland since the middle Holocene was reconstructed along a

northeast-to-southwest transect.

3.4. Dry bulk density, total organic carbon and nitrogen content

The dry bulk density (DBD) was measured using the oven-drying and weighing method (Loisel and Garneau, 2010), in which peat samples with a known volume (2 cm^3) were collected at 1 cm intervals, oven-dried at 105°C to a constant weight, and then weighed to calculate DBD. For total organic carbon (TOC) and total nitrogen (TN) analyses, the subsamples collected at 2 cm intervals were ground to <100 mesh, encapsulated in tin capsules, and analyzed using an elemental analyzer (Euro Vector EA3000). CAR was calculated using the following equation (Tolonen and Turunen, 1996):

$$\text{CAR} = \text{SR} \times \text{TOC} \times \text{DBD} \times 100 \quad (1)$$

where CAR represents the carbon accumulation rate ($\text{g C/m}^2/\text{yr}$), SR is the sediment rate (cm/yr), TOC is the total organic carbon content (%), and DBD is the dry bulk density (g/cm^3).

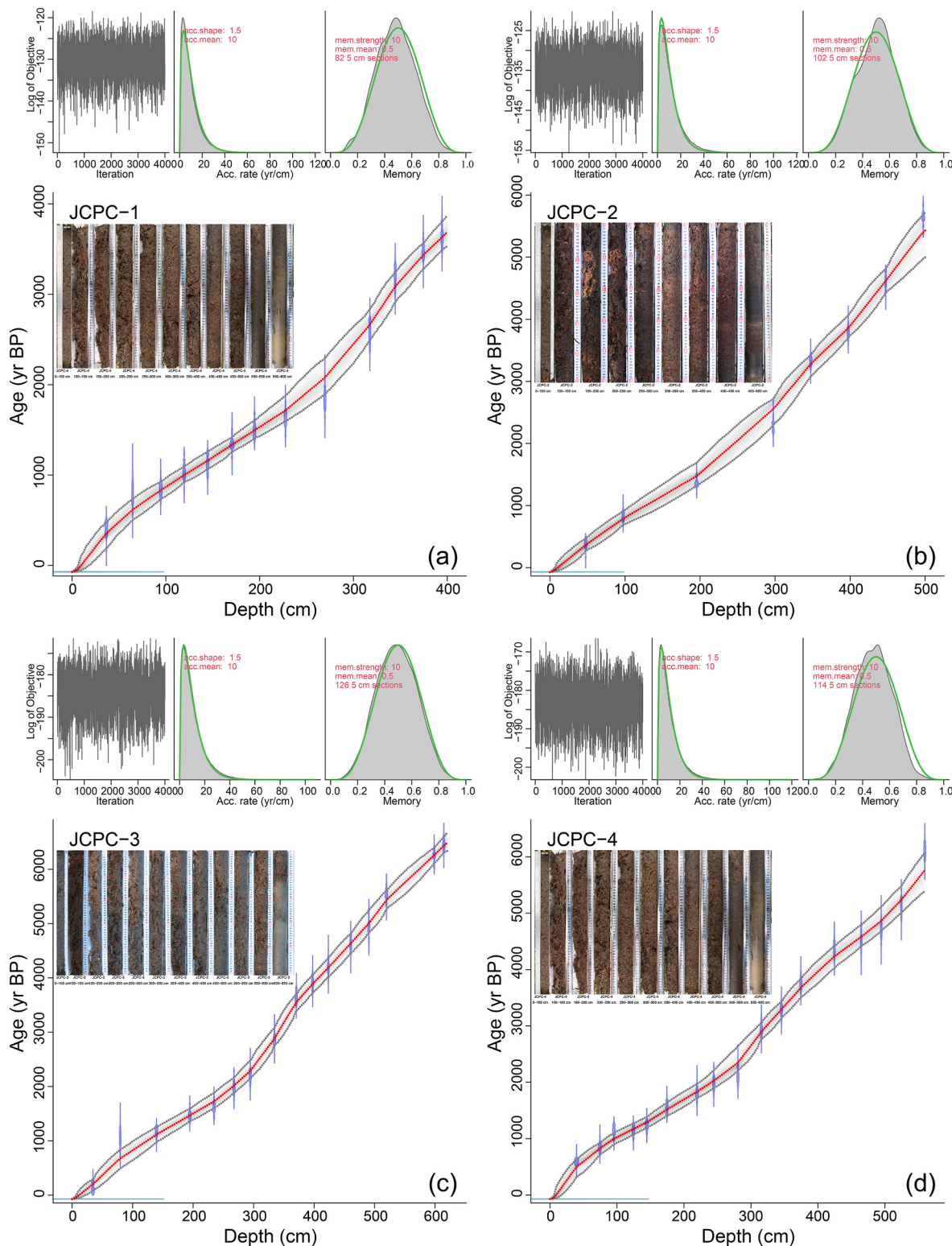


Fig. 2. Age-depth models produced using the Bacon approach for cores (a) JCPC-1, (b) JCPC-2, (c) JCPC-3, and (d) JCPC-4. The red lines show the weighted mean average, with gray shaded areas indicating the 95 % confidence intervals of the estimated age.

3.5. Cellulose extraction and carbon stable isotopes analysis

The extraction of α -cellulose and the analysis of carbon stable isotopes ($\delta^{13}\text{C}$) were conducted at 4 cm intervals across all cores. Approximately 2 cm^3 subsamples were initially rinsed with ultrapure water until fully dispersed, after which the above-ground residues of

Carex spp. were manually isolated under a stereomicroscope for the α -cellulose extraction. Extraction involved sequential digestion with sodium hydroxide (NaOH) and bleaching with sodium chlorite-glacial acetic acid ($\text{NaClO}_2\text{-CH}_3\text{COOH}$) (Daley, 2007). Following extraction, the samples were homogenized using a tissue homogenizer and freeze-dried at -80°C for 48 h. The $\delta^{13}\text{C}$ values were determined using

Table 1Radiocarbon dating (AMS¹⁴C) materials and results for cores JCPC-1, JCPC-2, JCPC-3 and JCPC-4.

Sample ID	Lab number	Depth (cm)	Material dated	¹⁴ C age (yr BP)	Error (yr)	Calibrated age ($\pm 2\sigma$, cal. yr BP)	Mean calibrated age (cal. yr BP)
JCPC-1-1	NENUR11283	36–37	<i>Carex</i> spp.	373	63	306–516	411
JCPC-1-2	NENUR11284	64–65	<i>Carex</i> spp.	861	126	627–1001	814
JCPC-1-3	NENUR11285	94–95	<i>Carex</i> spp.	937	66	723–958	841
JCPC-1-4	NENUR11286	119–120	Seed	1116	66	915–1179	1047
JCPC-1-5	NENUR11287	144–145	<i>Sphagnum</i> spp.	1203	65	973–1276	1125
JCPC-1-6	NENUR11288	170–171	<i>Carex</i> spp.	1440	65	1266–1421	1344
JCPC-1-7	NENUR11289	194–195	<i>Carex</i> spp.	1623	65	1364–1624	1494
JCPC-1-8	NENUR11290	227–228	<i>Carex</i> spp.	1742	65	1517–1798	1658
JCPC-1-9	NENUR11291	269–270	<i>Sphagnum</i> spp.	1920	74	1697–2003	1850
JCPC-1-10	NENUR11293	317–318	<i>Carex</i> spp.	2525	67	2410–2753	2582
JCPC-1-11	NENUR11294	344–345	Bulk sample	3017	66	3004–3368	3186
JCPC-1-12	NENUR11295	374–375	<i>Carex</i> spp.	3249	67	3351–3638	3495
JCPC-1-13	NENUR11296	394–395	<i>Carex</i> spp.	3393	67	3467–3778	3623
JCPC-2-1	NENUR10752	47–48	<i>Carex</i> spp.	326	52	295–494	395
JCPC-2-2	NENUR10753	97–98	<i>Carex</i> spp.	914	55	723–928	826
JCPC-2-3	NENUR10754	195–196	<i>Carex</i> spp.	1463	54	1285–1420	1353
JCPC-2-4	NENUR10756	297–298	<i>Carex</i> spp.	2293	55	2145–2434	2290
JCPC-2-5	NENUR10757	347–348	Seed	3129	55	3210–3455	3333
JCPC-2-6	NENUR10758	397–398	Seed	3516	57	3678–3930	3804
JCPC-2-7	NENUR10759	447–448	<i>Carex</i> spp.	4090	56	4505–4731	4618
JCPC-2-8	NENUR10761	497–498	Bulk sample	4910	60	5573–5754	5664
JCPC-3-1	NENUR11297	34–35	<i>Carex</i> spp.	74	63	7–152	80
JCPC-3-2	NENUR11298	79–80	<i>Carex</i> spp.	1126	134	779–1296	1038
JCPC-3-3	NENUR11299	139–140	<i>Carex</i> spp.	1254	65	1055–1297	1176
JCPC-3-4	NENUR11300	194–195	Seed	1587	67	1345–1605	1475
JCPC-3-5	NENUR11301	234–235	<i>Carex</i> spp.	1711	68	1468–1737	1603
JCPC-3-6	NENUR11302	267–268	<i>Carex</i> spp.	2024	66	1819–2148	1984
JCPC-3-7	NENUR11303	294–295	<i>Carex</i> spp.	2197	66	2045–2341	2193
JCPC-3-8	NENUR11304	334–335	<i>Carex</i> spp.	2743	66	2745–2998	2872
JCPC-3-9	NENUR11305	370–371	<i>Sphagnum</i> spp.	3394	67	3467–3779	3623
JCPC-3-10	NENUR11306	397–398	<i>Carex</i> spp.	3598	67	3714–4090	3902
JCPC-3-11	NENUR11307	423–424	<i>Sphagnum</i> spp.	3799	68	4062–4410	4236
JCPC-3-12	NENUR11308	460–461	<i>Sphagnum</i> spp.	4098	75	4502–4826	4664
JCPC-3-13	NENUR11309	490–491	<i>Carex</i> spp.	4330	72	4809–5073	4941
JCPC-3-14	NENUR11310	519–520	<i>Carex</i> spp.	4831	69	5448–5720	5584
JCPC-3-16	NENUR11312	598–599	<i>Carex</i> spp.	5467	70	6171–6403	6287
JCPC-3-17	NENUR11313	614–615	Seed	5665	70	6306–6572	6439
JCPC-4-1	NENUR11382	39–40	<i>Sphagnum</i> spp.	584	70	512–666	589
JCPC-4-2	NENUR11383	74–75	<i>Carex</i> spp.	942	67	721–960	841
JCPC-4-3	NENUR11384	95–96	<i>Sphagnum</i> spp.	1219	63	1050–1284	1167
JCPC-4-4	NENUR11385	124–125	<i>Carex</i> spp.	1229	67	1050–1289	1170
JCPC-4-5	NENUR11386	144–145	<i>Sphagnum</i> spp.	1333	68	1172–1353	1263
JCPC-4-6	NENUR11387	174–175	<i>Carex</i> spp.	1662	68	1401–1705	1553
JCPC-4-7	NENUR11388	219–220	<i>Carex</i> spp.	1883	66	1694–1945	1820
JCPC-4-8	NENUR11389	244–245	<i>Carex</i> spp.	2031	70	1818–2152	1985
JCPC-4-9	NENUR11390	280–281	<i>Carex</i> spp.	2131	69	1942–2320	2131
JCPC-4-10	NENUR11391	315–316	<i>Carex</i> spp.	2816	68	2766–3079	2923
JCPC-4-11	NENUR11392	345–346	<i>Carex</i> spp.	3088	70	3142–3451	3297
JCPC-4-12	NENUR11393	374–375	<i>Carex</i> spp.	3481	69	3569–3922	3746
JCPC-4-13	NENUR11394	424–425	<i>Carex</i> spp.	3941	71	4152–4574	4363
JCPC-4-14	NENUR11395	464–465	<i>Sphagnum</i> spp.	4029	87	4290–4736	4513
JCPC-4-15	NENUR11396	494–495	<i>Sphagnum</i> spp.	4181	89	4505–4878	4692
JCPC-4-16	NENUR11397	524–525	<i>Sphagnum</i> spp.	4484	90	4863–5322	5093
JCPC-4-17	NENUR11398	559–560	Bulk sample	5330	93	5927–6290	6109

an Isotope Mass Spectrometer (Thermo Fisher-Delta V Advantage) with L-glutamic acid ($\text{C}_5\text{H}_9\text{NO}_4$; $\delta^{13}\text{C} = -26.69\text{ ‰}$) as the reference standard. The analytical precision based on replicate analyses was $<0.15\text{ ‰}$.

4. Results

4.1. Age-depth model and peat accumulation rate

The age-depth models indicated that the basal ages of peat in cores JCPC-1, JCPC-2, JCPC-3, and JCPC-4 were 3.6, 5.7, 6.5, and 6.1 kyr BP, respectively, corresponding to temporal resolutions of 9.4, 11.6, 10.6, and 10.4 years (Fig. 2). The mean sediment rate (SR) across the JC peatland demonstrated limited variability, generally fluctuating around 0.1 cm/yr. JCPC-1 exhibited the highest mean SR at 0.12 cm/yr, with the range of 0.06–0.33 cm/yr, while JCPC-3 and JCPC-4 displayed the SR ranges of 0.05–0.33 cm/yr and the means of 0.10 and 0.11 cm/yr,

respectively. JCPC-2 showed the lowest mean SR at 0.09 cm/yr, ranging from 0.06 to 0.25 cm/yr (Fig. 4a). All the cores presented similar temporal patterns in SR, with the relatively stable fluctuations between 6.5 and 2.5 kyr BP, followed by an acceleration phase beginning at 2.5 kyr BP, peaking between 1.5 and 1 kyr BP, and then declining synchronously around 1.0 kyr BP (Fig. 4a).

4.2. Paleotopography and surface elevation evolution

The current surface elevation of the JC peatland varies by approximately 15 m and gradually decreases from north to south (Fig. 3b). Peat thickness ranged from 30 to 900 cm, with a mean of 210 cm, and exhibited a spatial distribution pattern that was higher in the northeast and lower in the southwest (Fig. 3c). The basal elevation displayed a pattern similar to that of peat thickness, with core JCPC-1 having the highest basal elevation and core JCPC-3 situated in the lowest-lying area

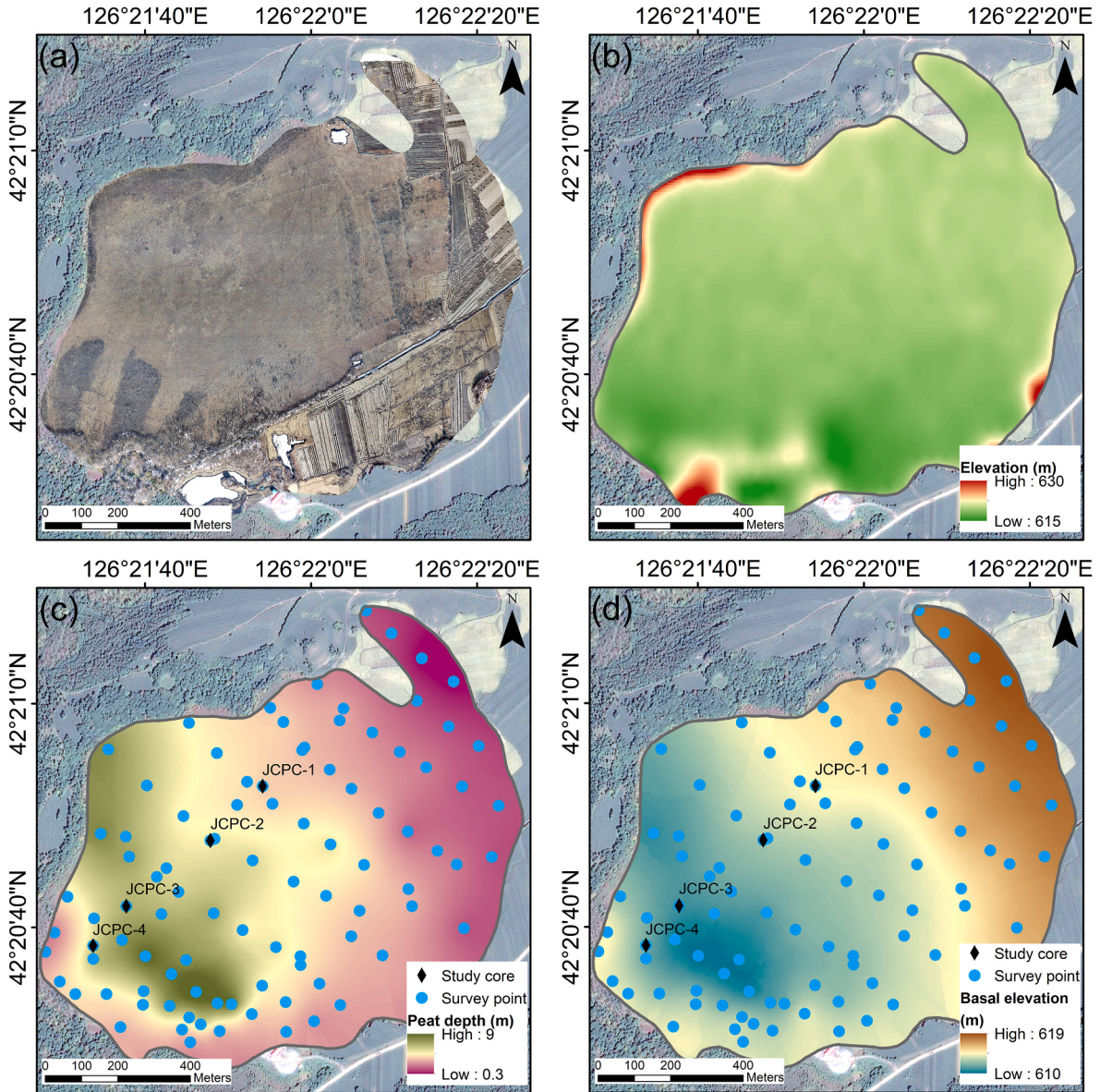


Fig. 3. (a) Remote sensing image of the JC peatland. (b-d) Surface elevation, peat thickness, and basal elevation of the JC peatland.

(Fig. 3d). Overall, the hydraulic gradient and surface elevation differences within the JC peatland demonstrated a gradually decreasing trend over the past 6.5 kyr, with JCPC-3 consistently representing the lowest elevation among the four study cores (Fig. 5).

4.3. Carbon accumulation rate

The DBD of JCPC-1 and JCPC-2 showed the similar characteristics, with mean values of 0.13 and 0.14 g/cm³, ranging from 0.03 to 0.48 and 0.03–0.50 g/cm³, respectively. JCPC-3 and JCPC-4 displayed the lower mean DBD values of 0.10 g/cm³, with the ranges of 0.03–0.16 and 0.01–0.19 g/cm³, respectively. Temporally, the high DBD values occurred before 2.5 kyr BP, followed by a decline and a recovery phase around 1.5 kyr BP (Fig. 4b). The TOC content in JCPC-2 and JCPC-3 averaged 45.0 % with ranges of 17.3–51.5 % and 29.7–55.5 %, respectively. JCPC-1 and JCPC-4 shared identical mean TOC values of 44.5 % with ranges of 24.9–54.6 % and 23.0–53.9 %, respectively. During 6.5–5.5 kyr BP, JCPC-3 maintained higher TOC concentrations than JCPC-4, whereas all the cores exhibited a synchronous TOC decline after 5.5 kyr BP (Fig. 4c). The mean TN content across all cores was 2.1

% with the variation ranges of 0.95–2.6 % (JCPC-1), 0.98–2.6 % (JCPC-2), 1.2–2.9 % (JCPC-3), and 1.4–2.8 % (JCPC-4), mirroring TOC trends (Fig. 4d). The C/N ratios showed limited spatial variability with JCPC-1 (21.3) and JCPC-2 (21.4) slightly exceeding JCPC-3 and JCPC-4 (both 21.1), and the peaks observed during 5.0–3.5 and 1.5–0.8 kyr BP (Fig. 4e).

JCPC-1 exhibited the highest mean CAR at 62.9 g C/m²/yr (range: 24.1–119 g C/m²/yr), followed by JCPC-2 with the mean of 53.4 g C/m²/yr (range: 21.9–103.5 g C/m²/yr), JCPC-3 showed the lowest mean CAR at 44.2 g C/m²/yr but with the widest range (14.4–154.4 g C/m²/yr), and JCPC-4 presented the moderate mean CAR of 47.7 g C/m²/yr and the most constrained range (18.8–88.2 g C/m²/yr). These values and their variation reflected the spatial heterogeneity in CAR across the JC peatland prior to 1.5 kyr BP, whereas all the cores displayed the nearly identical CAR trends over the last 1.5 kyr BP, marked by progressive declines culminating in peak values between 1.5 and 0.8 kyr BP (Fig. 4f).

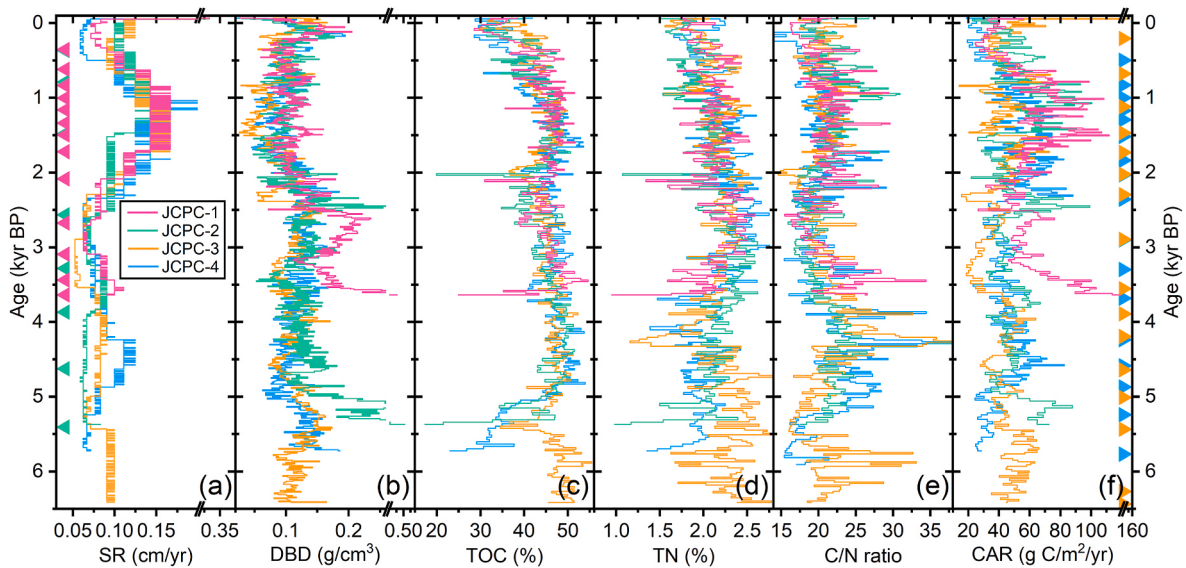


Fig. 4. Peat characteristics of cores JCPC-1, JCPC-2, JCPC-3, and JCPC-4. (a) Peat sediment rate (SR). (b) Dry bulk density (DBD). (c) Total organic carbon (TOC). (d) Total nitrogen (TN). (e) Carbon/nitrogen ratio (C/N ratio). (f) Carbon accumulation rate (CAR). The pink, olive, orange, and blue lines correspond to sediment cores JCPC-1, JCPC-2, JCPC-3, and JCPC-4, respectively, while the associated triangular markers denote the AMS ^{14}C dating points for each respective core.

4.4. Carbon stable isotopes

The mean $\delta^{13}\text{C}$ values of JCPC-1, JCPC-2, JCPC-3, and JCPC-4 were -26.1 ‰ , -25.2 ‰ , -26.4 ‰ , and -25.8 ‰ , respectively, with the ranges of -28.4 ‰ to -23.4 ‰ , -27.8 ‰ to -23.0 ‰ , -28.5 ‰ to -23.5 ‰ , and -28.9 ‰ to -22.4 ‰ . JCPC-1 showed a progressive $\delta^{13}\text{C}$ increase over the last 3.6 kyr (Fig. 6a). JCPC-2 exhibited a gradual increase prior to 1.5 kyr BP, followed by depletion around 1.5 kyr BP with minimum values during 1.5–1.0 kyr BP (Fig. 6b). JCPC-3 maintained relatively low $\delta^{13}\text{C}$ before 5.0 kyr BP, shifted to a decreasing trend during 5.0–1.5 kyr BP, and demonstrating the fluctuating increases over the last 1.5 kyr (Fig. 6c). JCPC-4 recorded the lowest values during 6.0–3.5 kyr BP, followed by a progressive decrease with recent lows in the last 1.5 kyr (Fig. 6d). The $\delta^{13}\text{C}$ variation in JCPC-3 differed from that in other cores, notably showing a decreasing trend from 4.5 to 2.0 kyr BP, while others displayed increasing trends during this interval. Overall, all four cores in the JC peatland demonstrated a millennial-scale increasing trend, with the most pronounced rise occurring after 1.5 kyr BP (Fig. 6).

5. Discussion

5.1. Moisture condition evolution in the JC peatland indicated by $\delta^{13}\text{C}$

The $\delta^{13}\text{C}$ values of vascular plants remaining from peat deposits serve as reliable proxies for reconstructing surface moisture conditions in peatlands (Hong et al., 2001; Amesbury et al., 2015; Dong et al., 2024). Under wet conditions, increased stomatal conductance facilitates greater ^{12}C assimilation, resulting in lower $\delta^{13}\text{C}$ values. In contrast, in drier environments, reduced stomatal apertures minimize water loss, enhance ^{13}C enrichment, and lead to higher $\delta^{13}\text{C}$ values (Ménot and Burns, 2001; Lin, 2013). According to this theory, higher $\delta^{13}\text{C}$ values are interpreted as indicative of drier surface conditions, whereas lower $\delta^{13}\text{C}$ values suggest more humid conditions within the JC peatland.

At millennial timescales, $\delta^{13}\text{C}$ values from the four peat cores in the JC peatland exhibited consistent trends, indicating an overall decrease in surface moisture (Fig. 7b, d, 7f, and 7h). This pattern is consistent with the existing paleoprecipitation and humidity reconstructions from the Changbai Mountains (Fig. 7b, d, 7f, 7h, and 7i–7k) (Chen et al., 2014; Stebich et al., 2015; Xu et al., 2019) and the intensity of the East Asian summer monsoon (EASM) (Fig. 7n) (Hu et al., 2008). Records

from the Sihailongwan and Xiaolongwan Maars demonstrated a fluctuating drying trend over the past 6.5 kyr (Fig. 7i and j) (Stebich et al., 2015; Xu et al., 2019). Although the Gushantun peatland reconstruction suggested increased moisture after 3 kyr BP, it also reflected a long-term decline in precipitation over the same period (Leng, 2019). Similar drying patterns were also observed in the $\delta^{13}\text{C}$ sequences of sediments from Jingpo Lake (Fig. 7k) (Chen et al., 2014). Although previous studies have indicated that peatland surface moisture can be influenced by temperature, where rising temperatures enhance evaporation and lead to drier conditions (Barber et al., 2000; Barber and Langdon, 2007), temperature reconstructions from the Hani peatland and Sihailongwan Maar Lake show that both the mean annual temperature and the temperature of the warmest month in the Changbai Mountains have declined over the past 6.5 kyr (Fig. 7l and m) (Stebich et al., 2015; Zheng et al., 2017). Despite this temperature decrease, the surface moisture in the JC peatland did not increase (Fig. 7b, d, 7f, and 7h), suggesting that its evolution is primarily controlled by regional precipitation rather than regional temperature.

Differences in surface moisture conditions across various locations within the JC peatland on a centennial timescale have also been documented. During 4.5–2.0 kyr BP, while most areas of the JC peatland exhibited a drying trend (Fig. 7b, d, and 7h), JCPC-3 showed a gradual moistening pattern, primarily because of its position as the lowest-lying area over the past 6.5 kyr, which facilitated water convergence and sustained relatively high humidity (Fig. 7f). Owing to its proximity to JCPC-3, JCPC-4 also displayed an increasing humidity trend between 3.2 and 2.0 kyr BP. Among the four cores, JCPC-4 exhibited the most frequent fluctuations in moisture conditions (Fig. 7h), likely because it was located near the peatland margins, where the water table levels varied more frequently (Charman, 2002; Loisel et al., 2013). In contrast, JCPC-1 and JCPC-2, situated in the intermediate zone between the center and edge of the peatland (Fig. 5), showed moderate surface humidity conditions and exhibited nearly identical humidity change patterns during the same period (Fig. 7b and d).

In summary, driven by precipitation and humidity variations in the Changbai Mountains, the JC peatland exhibited a long-term drying trend during the middle Holocene. On a centennial timescale, spatial heterogeneity in humidity evolution was evident across different locations, with the sedimentary center consistently maintaining relatively high moisture levels despite the regional precipitation decline, while the peatland margins experienced more frequent dry-wet alternations.

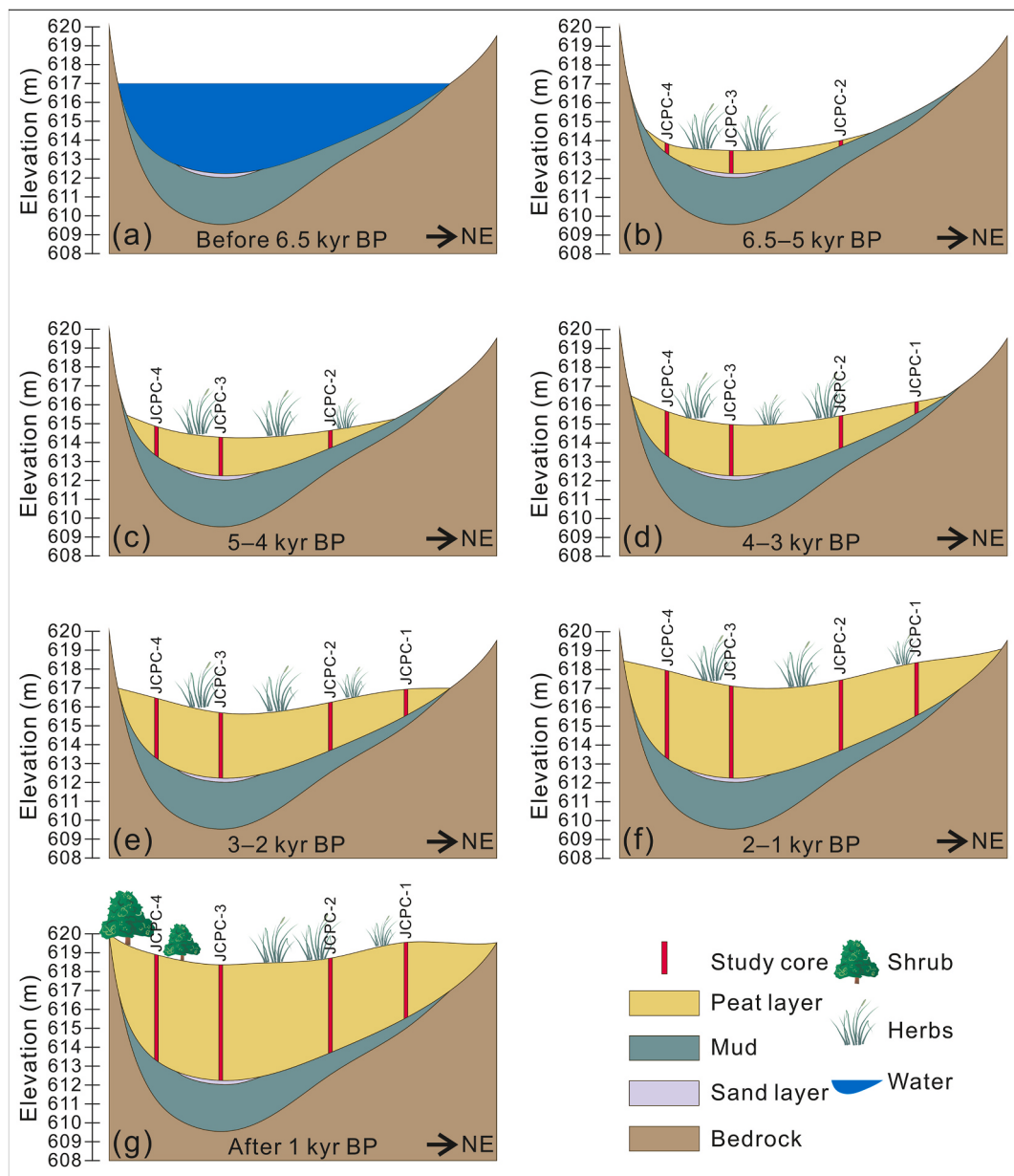


Fig. 5. Schematic diagram showing the evolution process of surface elevation in the JC peatland. The inferences are based on current surface elevation, peat depth, depth of the underlying mud layer, and sediment rates from four study cores.

5.2. Spatially heterogeneous characteristics of CAR in the JC peatland

Certain climatic factors, including summer insolation, summer-winter climate seasonality, and regional precipitation and temperature, are the predominant drivers of long-term CAR in peatlands (Jone and Yu, 2010; Zhao et al., 2014; Charman et al., 2013, 2015; Gallego-Sala et al., 2018). When solely influenced by external climatic factors, the carbon accumulation process at different locations within peatlands is expected to exhibit a consistent pattern of variation. However, during 6.5–1.5 kyr BP, the CAR at different locations within the JC peatland exhibited spatial heterogeneity. For example, during 5.5–4.0 kyr BP, JCPC-2 showed a declining CAR trend, whereas JCPC-4 displayed an opposite pattern. Between 4.0 and 1.5 kyr BP, JCPC-3, and JCPC-4 exhibited overall increasing CAR trends, whereas JCPC-1 and JCPC-2 experienced fluctuating declines (Fig. 7a, c, 7e, and 7g). Meanwhile, summer insolation, climate seasonality, EASM, and regional precipitation and temperature in the Changbai Mountains showed a general decreasing trend during this period (Fig. 7l, m, 7n, 7o, and 7p) (Hu et al.,

2008; Laskar et al., 2011; Stebich et al., 2015; Zheng et al., 2017). These observations suggest that, during the period from 6.5 to 1.5 kyr BP, in addition to climatic conditions, local environmental factors might have played an important role in regulating CAR variability.

To investigate the correlation between CAR at various locations in the JC peatland and its potential influencing factors, particularly surface moisture conditions, a detailed correlation analysis was conducted between CAR and the associated variables. The results revealed a negative correlation between $\delta^{13}\text{C}$ and CAR in cores JCPC-1, JCPC-2, and JCPC-4, indicating that greater surface moisture promoted higher CAR, whereas lower moisture inhibited CAR (Fig. 8). This relationship was primarily attributed to wet conditions that enhanced plant productivity and suppressed organic matter decomposition through the creation of anoxic environments (Lacourse and Davies, 2015; Panait et al., 2017). Similar patterns, where moist surface conditions could promote CAR, have also been observed in the Laolike (Dong et al., 2021), Hani (Cai et al., 2013), and Dongfanghong peatlands (Dong et al., 2024) of the Changbai Mountains.

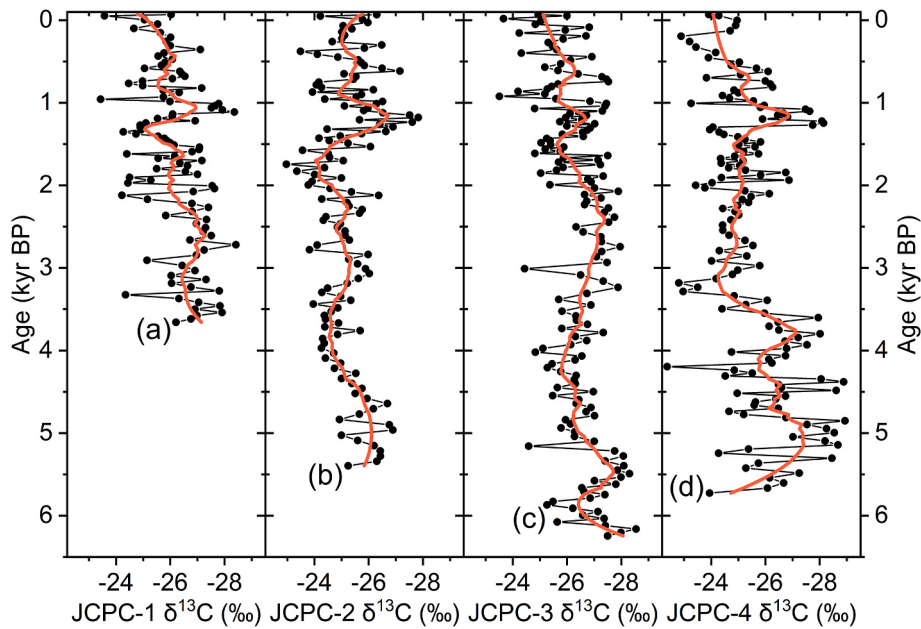


Fig. 6. Carbon stable isotopes ($\delta^{13}\text{C}$) of α -cellulose in *Carex* spp. remains for cores (a) JCPC-1, (b) JCPC-2, (c) JCPC-3, and (d) JCPC-4. The red line indicates the $\delta^{13}\text{C}$ after smoothing.

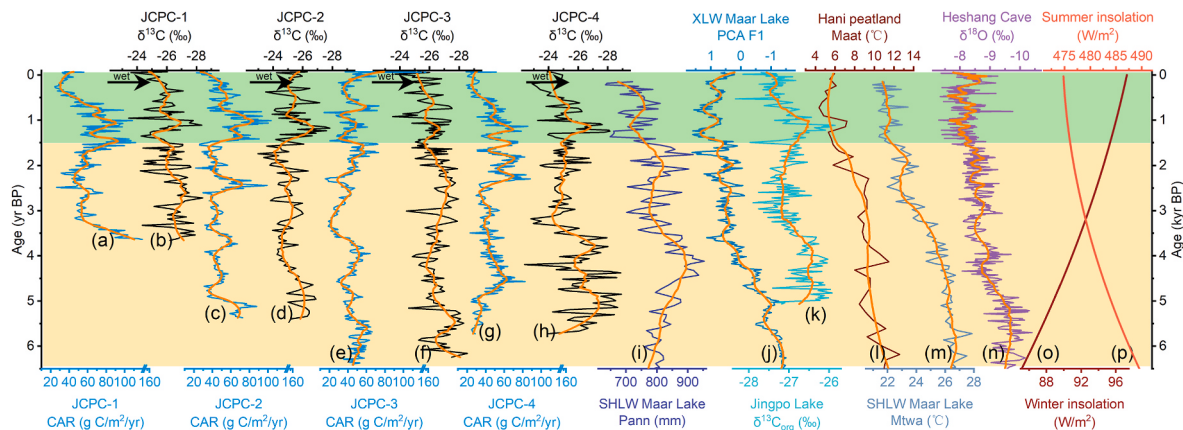


Fig. 7. Corresponding relationships between the carbon accumulation rate (CAR) and moisture conditions across different cores in the JC peatland, along with their comparisons with other regional paleoclimate records. CAR and $\delta^{13}\text{C}$ values for cores (a–b) JCPC-1, (c–d) JCPC-2, (e–f) JCPC-3, and (g–h) JCPC-4. (i) Reconstructed mean annual precipitation (Pann) from Sihailongwan (SHLW) Maar Lake (Stebich et al., 2015). (j) First principal component derived from principal component analysis (PCA F1) of the pollen record from the Xiaolongwan (XLW) Maar Lake (Xu et al., 2019). (k) The $\delta^{13}\text{C}_{\text{org}}$ record from Jingpo Lake (Chen et al., 2014). (l) Reconstructed mean annual temperature (Maat) in the Hani (HN) peatland (Zheng et al., 2017). (m) Reconstructed mean temperature of the warmest month (Mtwa) for the Sihailongwan (SHLW) Maar Lake (Stebich et al., 2015). (n) Oxygen isotope record from the Heshang Cave (Hu et al., 2008). (o–p) Summer and winter insolation curves at 50°N represented by the mean values for June and December, respectively (Laskar et al., 2011). The orange- and green-shaded areas in the background indicate the time intervals during which the carbon accumulation rate exhibited spatial heterogeneity and consistency, respectively.

For core JCPC-3, the positive correlation between CAR and surface moisture was not statistically significant (Fig. 8). During the period 4–1.5 kyr BP, a negative correspondence was observed between CAR and surface moisture (Fig. 7e and f). This phenomenon could primarily be attributed to the topographic position of the core and associated hydrological characteristics. Located at the lowest elevation (Fig. 5), JCPC-3 benefited from the elevated water tables sustained by inflow from surrounding areas, even during periods of reduced regional precipitation such as 4–2.5 kyr BP. However, prolonged waterlogging may reduce plant species diversity, constrain primary productivity and biomass, and thereby suppress CAR (Koirala et al., 2017). The observed increase in CAR during 2.5–1.5 kyr BP, coinciding with decreased surface moisture, could further support this hypothesis (Fig. 7e and f). Similar threshold effects of water level on CAR, where excessively high

water tables were detrimental, have been documented in Dajihu and Dongfanghong peatlands (Liu et al., 2022; Dong et al., 2024). Furthermore, frequent dry-wet fluctuations in core JCPC-4 may enhance peat decomposition and potentially influence the CAR-moisture relationship (Zhong et al., 2020; Dong et al., 2024). Conversely, CAR in JCPC-4 showed a significant positive correlation with surface moisture (Fig. 8). This suggested that despite frequent hydrological variability, the underlying relationship between surface moisture and CAR remained intact, and decomposition was likely not the dominant factor influencing CAR during this period (Charman et al., 2013). In contrast, cores JCPC-1 and JCPC-2, located at mid-slope positions, received stable hydrological inputs while avoiding prolonged waterlogging (Fig. 5), thus supporting a higher CAR.

In summary, the CAR of the JC peatland during the period 6.5–1.5

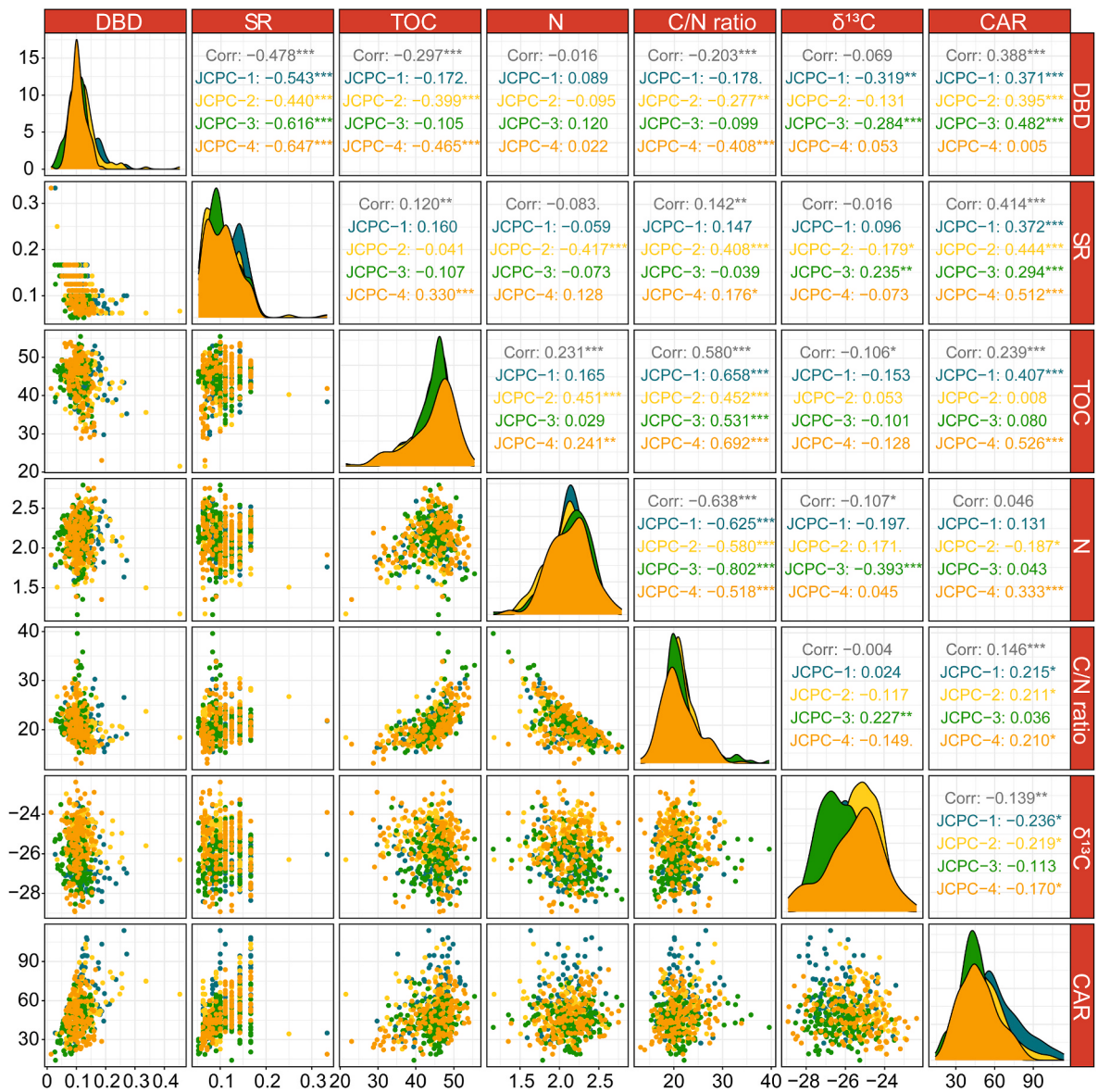


Fig. 8. Correlations between the carbon accumulation rate (CAR) of different cores in the JC peatland and dry bulk density (DBD), peat sediment rate (SR), total organic carbon content (TOC), nitrogen content (N), carbon/nitrogen (C/N) ratio, and $\delta^{13}\text{C}$.

kyr BP exhibited the spatial heterogeneity, with the regional climate not serving as the primary driver. Except for the central locations influenced by low-lying topography, CAR in the remaining areas showed a significant positive correlation with surface moisture, indicating that surface moisture conditions were the predominant influencing factor during this period.

5.3. Consistent CAR within the JC peatland and its response to climate change

The JC peatland exhibited a consistent decrease in CAR across different cores during the last 1.5 kyr (Fig. 7a, c, 7e, and 7g), corresponding to declining summer insolation, summer-winter climate seasonality (Fig. 7o and p) (Laskar et al., 2011), and regional temperatures in the Changbai Mountains (Fig. 7l and m) (Stebich et al., 2015; Zheng et al., 2017), suggesting potential climate-driven influences on carbon accumulation. This pattern primarily resulted from reduced photosynthetic rates due to diminished summer insolation and decreased mean annual and growing season temperatures, along with a contracted growing season caused by decreased climate seasonality (Nemani et al.,

2003; Jone and Yu, 2010; Charman et al., 2013; Gallego-Sala et al., 2018). These combined effects likely led to a reduction in net primary productivity (NPP), thereby limiting CAR. Additionally, the CAR trends during this period were closely aligned with regional precipitation and humidity patterns in the Changbai Mountains. For instance, the pollen data from Sihailongwan Maar Lake indicated significant precipitation declines during the last 1.5 kyr BP (Fig. 7i) (Stebich et al., 2015), consistent with the declining moisture indices from Xiaolongwan Maar Lake (Fig. 7j) (Xu et al., 2019). These findings highlight the persistent hydroclimatic controls on CAR in the JC peatland, likely driven by the reduced regional precipitation that lowered the peatland water table, resulting in moisture limitations on plant growth and subsequent suppression of NPP and CAR (Charman et al., 2015).

In addition to plant production, the degree of peat decomposition is a critical determinant of CAR (Charman, 2002; Ise et al., 2008; Dorrepaal et al., 2009; Yang et al., 2023), with the C/N ratio serving as an indicator. Higher values reflect lower decomposition levels (Kuhry and Vitt, 1996). In the JC peatland, the C/N ratios in all four cores showed a declining trend during the last 1.5 kyr (Fig. 4e), corresponding with increased decomposition rates and reduced CAR. Correlation analysis

revealed significant positive relationships between the C/N ratios and CAR in all cores, except for JCPC-3 (Fig. 8), indicating that the carbon accumulation process was influenced by decomposition. This was primarily attributed to reduced regional precipitation over the past 1.5 kyr, which likely lowered the water table, increased the thickness of the acrotelm, and enhanced the soil respiration and microbial activity, thereby accelerating the decomposition and decreasing the carbon sequestration (Gillooly et al., 2001; Ise et al., 2008; Dorrepaal et al., 2009). It is noteworthy that existing pollen and plant macrofossil studies indicate a gradual intensification of human impact on the study area after 1.5 kyr BP (Jiang et al., 2008). Consequently, the potential influence of human activities on CAR during this period cannot be entirely excluded, and related inferences should be interpreted with caution.

The consistent decline in carbon accumulation in the JC peatland over the last 1.5 kyr could mainly be attributed to the reduced summer solar insolation, the decreased summer-winter climate seasonality, and the decline in regional temperature and precipitation. Under these climatic conditions, vegetation production was constrained and the degree of peat decomposition increased.

5.4. Role of climate and local conditions in determining long-term carbon accumulation

The CAR of the JC peatland exhibited a consistent response to regional climate and was closely correlated with local hydrological conditions. The relationships among CAR, regional climate, and surface moisture at different locations indicated that the influence of regional climatic factors and local conditions on CAR varied across different stages of carbon accumulation.

During the early stage of carbon accumulation (6.5–1.5 kyr BP), under an overall declining trend in regional precipitation (Chen et al., 2014; Stebich et al., 2015; Xu et al., 2019), CAR at different locations within the JC peatland exhibited the divergent patterns for most of this period. This phenomenon may result from greater surface elevation differences and hydraulic gradients within the peatland during this interval (Fig. 5), which could modulate the impact of regional precipitation on local hydrological conditions, leading to spatial variations in surface moisture (Fig. 9a). In relatively wet locations (e.g., JCPC-3), CAR was constrained, whereas more favorable hydrological conditions promoted higher CAR at other sites (e.g., JCPC-1, JCPC-2, and JCPC-4). Moreover, during the continuous decline in both annual average and growing season temperatures (Fig. 7l and m) (Stebich et al., 2015; Zheng

et al., 2017), the CAR across the cores responded differently (Fig. 7a, c, 7e, and 7g). These observations suggested that the regional climate was not the primary driver of CAR during this period, whereas the local topography and hydrological conditions played a dominant role in regulating carbon accumulation.

During the later stage of carbon accumulation (after 1.5 kyr BP), the decreased CAR in the JC peatland coincided with a reduction in the regional precipitation in the Changbai Mountains (Fig. 7i–k) (Chen et al., 2014; Stebich et al., 2015; Xu et al., 2019) and the surface moisture within the peatland. This can primarily be attributed to the gradual decrease in surface elevation differences resulting from peat accumulation, which reduced the spatial variability in surface moisture and led to a more uniform response to regional precipitation across different locations (Fig. 9b). Furthermore, the influence of both the annual average temperature and growing season temperature on CAR intensified during this period (Fig. 7l and m) (Stebich et al., 2015; Zheng et al., 2017). The combined effects of reduced precipitation, lower temperatures, and diminished peatland moisture suppressed vegetation productivity, thereby lowering CAR (Jone and Yu, 2010; Charman et al., 2013). This convergence in CAR during later stages was also observed in other peatlands within the Changbai Mountains. For example, the Baijianghe peatland located 35 km from the JC peatland displayed spatial heterogeneity in CAR from 5 to 1.4 kyr BP, whereas the three investigated cores demonstrated nearly identical CAR values over the past 1.4 kyr BP (Dong et al., 2023). Similarly, in the Laolike peatland, the CAR values from the two different cores were largely aligned over the past 4 kyr BP (Dong et al., 2021). These findings collectively suggested that during the late stage of carbon accumulation, climate became the dominant control on CAR in peatlands as surface elevation and hydrological differences progressively diminished.

In general, during the initial stage of carbon accumulation in the JC peatland, the influence of regional precipitation on CAR was modulated by variations in the surface elevation and hydrological conditions, resulting in significant spatial heterogeneity. In contrast, during the later stages of carbon accumulation, as the differences in surface elevation gradually diminished, the spatial variability in hydrological conditions also decreased, leading to regional climate becoming the predominant factor influencing CAR.

6. Conclusion

This study investigated the mechanisms by which climatic factors

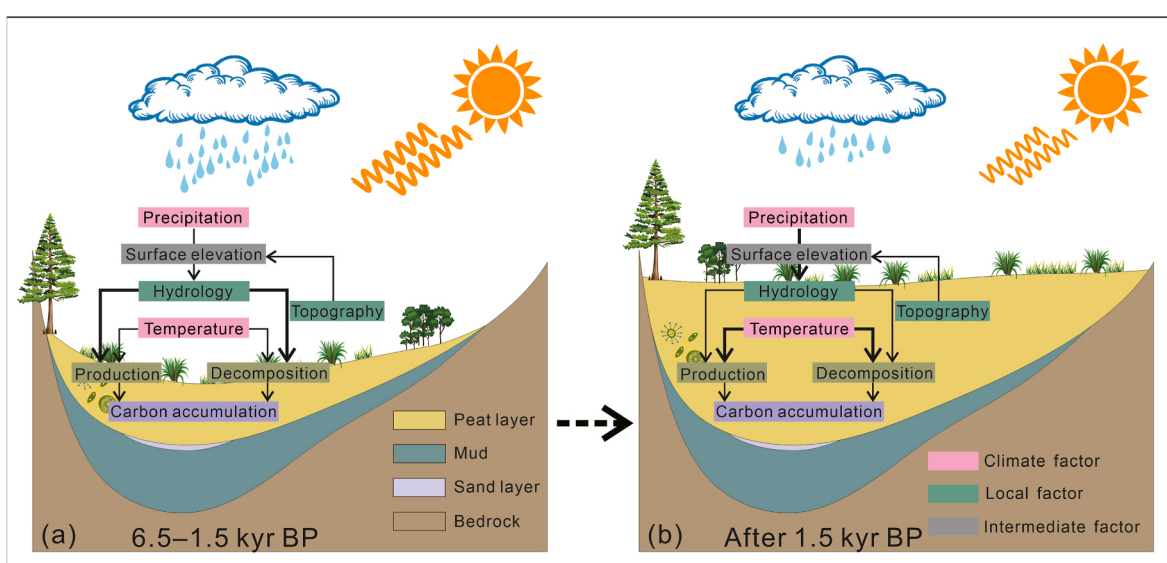


Fig. 9. Schematic diagram showing driving factors of spatial heterogeneity and consistency in the carbon accumulation process of the JC peatland.

and local conditions could influence the spatial heterogeneity and consistency of CAR within the JC peatland. The reconstructed surface moisture across different locations within the JC peatland demonstrated a general millennial-scale decline that was primarily driven by regional precipitation in the Changbai Mountains. From 6 to 1.5 kyr BP, CAR exhibited spatial heterogeneity, with local hydrological conditions emerging as the predominant influencing factor. This was attributed to the surface elevation differences that redistributed regional precipitation to generate localized moisture gradients and amplify the role of local moisture in modulating CAR. Prolonged saturation was found to inhibit carbon accumulation, revealing the presence of an optimal moisture threshold for CAR, as evidenced by the significant correlation between surface moisture and CAR under moderate moisture conditions. A pronounced convergence in CAR patterns emerged after 1.5 kyr BP, as climatic factors became the dominant control, surpassing local influences. This shift was driven by the diminished surface elevation gradients that led to a uniform moisture decline under reduced precipitation, along with the falling regional temperatures that constrained vegetation productivity and CAR. Overall, this study demonstrated that CAR in peatlands was not only governed by climate, but that the spatial heterogeneity in local conditions resulted in varied responses to climate change, even within the same peatland. These findings advance the mechanistic understanding of carbon accumulation processes in peatlands and provide a robust scientific foundation for assessing their carbon sequestration potential under future climate change scenarios.

Author contributions

Yanmin Dong: Conceptualization, Project administration, Investigation, Formal analysis, Writing – original draft, Funding acquisition. Jing Li: Formal analysis. Sizhu Li: Formal analysis, Investigation. Lu Yu: Formal analysis, Investigation. Zhiwei Xu: Validation, con-editing. Shengzhong Wang: Supervision, Project administration, Methodology, Funding acquisition.

Declaration of competing interest

The authors declare that they have no known competing financial interests or personal relationships that could have appeared to influence the work reported in this paper.

Acknowledgments

We are grateful to engineer Liu Shanshan and Liu Ziping from Northeast Normal University for the laboratory work. This research was jointly supported by the National Key Research and Development Program of China (2023YFF0806900), the Fundamental Research Funds for the Central Universities (2412023QD024), the National Natural Science Foundation of China (32241033, 42494822, U23A2003). The editor and the anonymous reviewers are thanked for their comments that improved the quality of this manuscript.

Appendix A. Supplementary data

Supplementary data to this article can be found online at <https://doi.org/10.1016/j.quascirev.2025.109581>.

Data availability

All data and/or code is contained within the submission.

References

- Amesbury, M.J., Charman, D.J., Newnham, R.M., Loader, N.J., Goodrich, J.P., Royles, J., Campbell, D.I., Roland, T.P., Gallego-Sala, A.V., 2015. Carbon stable isotopes as a palaeoclimate proxy in vascular plant dominated peatlands. *Geochem. Cosmochim. Acta* 164, 161–174.
- Barber, K.E., Langdon, P.G., 2007. What drives the peat-based palaeoclimate record? A critical test using multi-proxy climate records from northern Britain. *Quat. Sci. Rev.* 26, 3318–3327.
- Barber, K.E., Maddy, D., Rose, N., Stevenson, A.C., Stoneman, R., Thompson, R., 2000. Replicated proxy-climate signals over the last 2000 yr from two distant UK peat bogs: new evidence for regional palaeoclimate teleconnections. *Quat. Sci. Rev.* 19, 481–487.
- Blaauw, M., Christen, J.A., Lopez, A.M.A., Vazquez, J.E., Gonzalez, V.O.M., Belding, T., Theiler, J., Gough, B., Karney, C., 2019. Rbacon: Age-Depth modelling using Bayesian Statistics. <https://CRAN.R-project.org/package=rbacon>.
- Blaauw, M., Christen, J.A., 2011. Flexible paleoclimate age-depth models using an autoregressive gamma process. *Bayesian Anal.* 6 (3), 457–474.
- Bronk, R.C., 2009. Bayesian analysis of radiocarbon dates. *Radiocarbon* 51, 337–360.
- Cai, C., Hong, B., Zhu, Y.X., Hong, Y.T., Wang, Y., Peng, H.J., 2013. Holocene peat accumulation rates and influence factors from the Hani peatland, Northeast China. *Earth Environ.* 41, 597–604 (in Chinese).
- Charman, D.J., 2002. Peatlands and Environment Change. John Wiley, New York.
- Charman, D.J., Amesbury, M., Hinchliffe, W., Hughes, P.D.M., Mallon, G., Blake, W.H., Daley, T.J., Gallego-Sala, A.V., Mauquoy, D., 2015. Drivers of Holocene peatland carbon accumulation across a climate gradient in northeastern North America. *Quat. Sci. Rev.* 121, 110–119.
- Charman, D.J., Beilman, D.W., Blaauw, M., Booth, R.K., Brewer, S., Chambers, F.M., Christen, J.A., Gallego-Sala, A.V., Harrison, S.P., Hughes, P.D.M., Jackson, S.T., Korhola, A., Mauquoy, D., Mitchell, F.J.G., Prentice, I.C., van der Linden, M., Vleeschouwer, F.D., Yu, Z.C., Alm, J., Bauer, I.E., Corish, Y.M.C., Garneau, M., Hohl, V., Huang, Y., Karofeld, E., Roux, G.L., Loisel, J., Moschen, R., Nichols, J.E., Nieminen, T.M., MacDonald, G.M., Phadtare, N.R., Rausch, N., Sillasoo, Ü., Swindles, G.T., Tuittila, E.S., Ukonmaanaho, L., Välimäki, M., van Bellen, S., van Geel, B., Vitt, D.H., Zhao, Y., 2013. Climate-related changes in peatland carbon accumulation during the last millennium. *Biogeosciences* 10, 929–944.
- Chen, R., Shen, J., Li, C.H., Zhang, E.L., Sun, W.W., Ji, M., 2014. Mid- to late-Holocene East Asian summer monsoon variability recorded in lacustrine sediments from Jingpo Lake, Northeastern China. *Holocene* 25, 454–468.
- Daley, T.J., 2007. Tracking Holocene Climate Change Using Peat Bog Stable Isotopes. University of Southampton.
- De Vleeschouwer, F., Chambers, F.M., Swindles, G.T., 2010. Coring and sub-sampling of peatlands for palaeoenvironmental research. *Mires Peat* 7, 1–10.
- Dong, Y.M., Li, H.K., He, H.S., Wang, S.Z., 2021. Holocene peatland development, carbon accumulation and its response to climate forcing and local conditions in Laolike peatland, northeast China. *Quat. Sci. Rev.* 268, 107124.
- Dong, Y.M., Li, H.K., Wang, S.Z., He, H.S., 2023. The development process of a temperate montane peatland and its controlling factors since the middle Holocene. *Sci. China Earth Sci.* 66 (3), 594–608.
- Dong, Y.M., Li, H.K., Xu, Z.W., Yu, L., Yang, Y.H., Wang, S.Z., 2024. Development and carbon accumulation dynamics of a minerotrophic fen during the last millennium, northeast China. *Catena* 240, 107976.
- Dorrepael, E., Toet, S., van Logtestijn, R.S.P., Swart, E., van de Weg, M.J., Callaghan, T.V., Aerts, R., 2009. Carbon respiration from subsurface peat accelerated by climate warming in the subarctic. *Nature* 460 (7255), 616–619.
- Feurdean, A., Galka, M., Florescu, G., Diaconu, A.C., Tanjău, I., Kirpotin, S., Hutchinson, S.M., 2019. 2000 years of variability in hydroclimate and carbon accumulation in western Siberia and the relationship with large-scale atmospheric circulation: a multi-proxy peat record. *Quat. Sci. Rev.* 226, 105948.
- Frolking, S.E., Roulet, N.T., 2007. Holocene radiative forcing impact of northern peatland carbon accumulation and methane emissions. *Glob. Change Biol.* 13, 1079–1088.
- Gallego-Sala, A.V., Charman, D.J., Brewer, S., Page, S.E., Prentice, I.C., Friedlingstein, P., Moreton, S., Amesbury, M.J., Beilman, D.W., Björck, S., Blyakharchuk, T., Bochicchio, C., Booth, R.K., Bunbury, J., Camill, P., Carless, D., Chimner, R.A., Clifford, M., Cressey, E., Courtney-Mustaphi, C., Francois, D.V., de Jong, R., Fialkiewicz-Koziel, B., Finkelstein, S.A., Garneau, M., Githumbi, E., Hribaljan, J., Holmqvist, J., Hughes, P.D.M., Jones, C., Jones, M.C., Karofeld, E., Klein, E.S., Kokfelt, U., Korhola, A., Lacourte, T., Roux, G.L., Lamentowicz, M., Large, D., Lavoie, M., Loisel, J., Mackay, H., MacDonald, G.M., Makila, M., Magnan, G., Marchant, R., Marcisz, K., Cortizas, A.M., Massa, C., Mathijssen, P., Mauquoy, D., Michall, T., Mitchell, F.J.G., Moss, P., Nichols, J., Oksanen, P.O., Orme, L., Packalen, M.S., Robinson, S., Roland, T.P., Sanderson, N.K., Sannel, A.B.K., Silva-Sánchez, N., Steinberg, N., Swindles, G.T., Turner, T.E., Uglow, J., Välimäki, M., van Bellen, S., van der Linden, M., van Geel, B., Wang, G.P., Yu, Z.C., Zaragoza-Castells, J., Zhao, Y., 2018. Latitudinal limits to the predicted increase of the peatland carbon sink with warming. *Nat. Clim. Change* 8, 907–913.
- Gillooly, J.F., Brown, J.H., West, G.B., Savage, V.M., Charnov, E.L., et al., 2001. Effect of size and temperature on metabolic rate. *Science* 293, 2248–2251.
- Hong, Y.T., Wang, Z.G., Jiang, H.B., Lin, Q.H., Hong, B., Zhu, Y.X., Wang, Y., Xu, L.S., Leng, X.T., Li, H.D., 2001. A 6000-year record of changes in drought and precipitation in northeastern China based on a $\delta^{13}\text{C}$ time series from peat cellulose. *Earth Planet Sci. Lett.* 185 (1), 111–119.
- Hu, C.Y., Henderson, G.M., Huang, J.H., Xie, S.C., Sun, Y., Johnson, K.R., 2008. Quantification of Holocene asian monsoon rainfall from spatially separated cave records. *Earth Planet Sci. Lett.* 266, 221–232.
- Huang, Y.Y., Ciais, P., Luo, Y.Q., Zhu, D., Wang, Y.P., Qiu, C.J., Goll, D.S., Guenet, B., Makowski, D., Graaf, I.D., Leifeld, J., Kwon, M.J., Hu, J., Qu, L.Y., 2021. Tradeoff of CO₂ and CH₄ emissions from global peatlands under water-table drawdown. *Nat. Clim. Change* 11, 618–622.

- Ise, T., Dunn, A.L., Wofsy, S.C., Moorcroft, P.R., 2008. High sensitivity of peat decomposition to climate change through water-table feedback. *Nat. Geosci.* 1 (11), 763–766.
- Jiang, W.Y., Leroy, S.A.G., Ogle, N., Chu, G.Q., Wang, L., Liu, J.Q., 2008. Natural and anthropogenic forest fires recorded in the Holocene pollen record from a Jinchuan peat bog, northeastern China. *Palaeogeogr. Palaeoclimatol. Palaeoecol.* 261, 47–57.
- Jones, M.C., Yu, Z.C., 2010. Rapid deglacial and early Holocene expansion of peatlands in Alaska. *Proc. Natl. Acad. Sci. USA* 107, 7347–7352.
- Koirala, S., Jung, M., Reichstein, M., de Graaf, I.E.M., Camps-Valls, G., Ichii, K., Papale, D., Ráduly, B., Schwalm, C.R., Tramontana, G., Carvalhais, N., 2017. Global distribution of groundwater-vegetation spatial covariation. *Geophys. Res. Lett.* 44, 4134–4142.
- Kuhry, P., Vitt, D.H., 1996. Fossil carbon/nitrogen ratios as a measure of peat decomposition. *Ecology* 77, 271–275.
- LaCourse, T., Davies, M.A., 2015. A multi-proxy peat study of Holocene vegetation history, bog development, and carbon accumulation on northern Vancouver Island, Pacific coast of Canada. *Holocene* 25, 1165–1178.
- Laskar, J., Fienga, A., Gastineau, M., Manche, H., 2011. La2010: a new orbital solution for the long-term motion of the Earth. *Astron. Astrophys.* 532, A89.
- Leng, C.C., 2019. Phytolith record of high resolution climate change in Gushantun peatland since last Glacial Age. MS Thesis. Northeast Normal University, pp. 30–32 (in Chinese with English abstract).
- Lin, G.H., 2013. Stable Isotope Ecology. Higher education press, Beijing, pp. 367–417 (in Chinese).
- Li, H.Y., Gu, Y.S., Ge, J.W., Yu, Z.C., Xu, X.N., Zhang, Z.Q., Cheng, S.G., Xie, S.C., 2022. The response of the Dajiuhe Peatland ecosystem to hydrological variations: implications for carbon sequestration and peatlands conservation. *J. Hydrol.* 612, 128307.
- Loisel, J., Bellen, S.V., Pelletier, L., Talbot, J., Hugelius, G., Karra, D., Yu, Z.C., Nichols, J., Holmqvist, J., 2017. Insights and issues with estimating northern peatland carbon stocks and fluxes since the last glacial maximum. *Earth Sci. Rev.* 165, 59–80.
- Loisel, J., Garneau, M., 2010. Late Holocene paleoecohydrology and carbon accumulation estimates from two boreal peat bogs in eastern Canada: potential and limits of multi-proxy archives. *Palaeogeogr. Palaeoclimatol. Palaeoecol.* 291, 493–533.
- Loisel, J., Yu, Z.C., 2013. Holocene peatland carbon dynamics in Patagonia. *Quat. Sci. Rev.* 69, 125–141.
- Loisel, J., Yu, Z.C., Parsekian, A., Nolan, J., Slater, L., 2013. Quantifying landscape morphology influence on peatland lateral expansion using ground-penetrating radar (GPR) and peat core analysis. *J. Geophys. Res. Biogeosci.* 118, 373–384.
- Longman, J., Veres, D., Haliuc, A., Finsinger, W., Ersek, V., Pascal, D., Sava, T., Begy, R., 2021. Carbon accumulation rates of Holocene peatlands in central-eastern Europe document the driving role of human impact over the past 4000 years. *Clim. Past.* 17, 2633–2652.
- Mathijssen, P.J.H., Galka, M., Borken, W., Knorr, K.H., 2019. Plant communities control long term carbon accumulation and biogeochemical gradients in a Patagonian bog. *Sci. Total Environ.* 684 (20), 670–681.
- Mathijssen, P.J.H., Välijanta, M., Korrensalo, A., Alekseychik, P., Vesala, T., Rinne, J., Tuittila, E.S., 2016. Reconstruction of Holocene carbon dynamics in a large boreal peatlandcomplex, southern Finland. *Quat. Sci. Rev.* 142, 1–15.
- Ménot, G., Burns, S.J., 2001. Carbon isotopes in ombrogenic peat bog plants as climatic indicators, calibration from an altitudinal transect in Switzerland. *Org. Geochem.* 32, 233–245.
- Nemani, R.R., Keeling, C.D., Hashimoto, H., Jolly, W.M., Piper, S.C., Tucker, C.J., Myneni, R.B., Running, S.W., 2003. Climate-driven increases in global terrestrial net primary production from 1982 to 1999. *Science* 300, 1560–1563.
- Olsson, I., 1986. Radiometric methods. In: Berglund, B. (Ed.), *Handbook of Holocene Palaeoecology and Palaeohydrology*. John Wiley and Sons, Chichester, pp. 273–312.
- Panait, A., Diaconu, A., Galca, M., Grindean, R., Hutchinson, S.M., Hickler, T., Lamentowicz, M., Mulch, A., Tanjău, I., Werner, C., Feurdean, A., 2017.
- Hydrological conditions and carbon accumulation rates reconstructed from a mountain raised bog in the Carpathians: a multi-proxy approach. *Catena* 152, 57–68.
- Perrier, L., Garneau, M., Pratte, S., Sanderson, N.K., 2022. Climate-driven Holocene ecohydrological and carbon dynamics from maritime peatlands of the Gulf of St. Lawrence, eastern Canada. *Holocene* 32, 749–763.
- Piilo, S.R., Korhola, A., Heiskanen, L., Tuovinen, J.P., Aurela, M., Juutinen, S., Marttila, H., Saari, M., Tuittila, E.S., Turunen, J., Välijanta, M.M., 2020. Spatially varying peatland initiation, Holocene development, carbon accumulation patterns and radiative forcing within a subarctic fen. *Quat. Sci. Rev.* 248, 106596.
- Primeau, G., Garneau, M., 2021. Carbon accumulation in peatlands along a boreal to subarctic transect in eastern Canada. *Holocene* 31 (5), 858–869.
- Reimer, P.J., Austin, W.E.N., Bard, E., Bayliss, A., Blackwell, P.G., Ramsey, C.B., Butzin, M., Cheng, H., Edwards, R.L., Friedrich, M., Grootes, P.M., Guilderson, T.P., Hajdas, I., Heaton, T.J., Hogg, A.G., Hughen, K.A., Kromer, B., Manning, S.W., Muscheler, R., Palmer, J.G., Pearson, C., van der Plicht, J., Reimer, R.W., Richards, D.A., Scott, E.M., Southon, J.R., Turney, C.S.M., Wacker, L., Adolphi, F., Büntgen, U., Capatti, M., Fahrni, S.M., Fogtmann-Schulz, A., Friedrich, R., Köhler, P., Kudsk, S., Miyake, F., Olsen, J., Reinig, F., Sakamoto, M., Sookdeo, A., Talamo, S., 2020. The IntCal20 Northern Hemisphere radiocarbon age calibration curve (0–55 cal kBP). *Radiocarbon* 62, 725–757.
- Robitaille, M., Garneau, M., van Bellen, S., Sanderson, N.K., 2021. Long-term and recent ecohydrological dynamics of patterned peatlands in north-central Quebec (Canada). *Holocene* 31 (5), 844–857.
- Rydin, H., Jeglum, J.K., Hooijer, A., 2006. *The Biology of Peatlands, the Biology of Habitats*. Oxford University Press, Oxford, New York.
- Stebich, M., Rehfeld, K., Schlüter, F., Tarasov, P.E., Liu, J.Q., Mingram, J., 2015. Holocene vegetation and climate dynamics of NE China based on the pollen record from Shihailongwan Maar lake. *Quat. Sci. Rev.* 124, 275–289.
- Tolonen, K., Turunen, J., 1996. Accumulation rates of carbon in mires in Finland and implications for climate change. *Holocene* 6, 171–178.
- van Bellen, S., Shotyk, W., Magnan, G., Davies, L., Mullan-Boudreau, G., Garneau, M., Noemberg, T., Bragazza, L., Zaccione, C., 2020. Carbon and nitrogen accumulation rates in ombrotrophic peatlands of central and northern Alberta, Canada, during the last millennium. *Biogeochemistry* 151, 251–272.
- Xing, W., Bao, K.S., Guo, W.Y., Lu, X.G., Wang, G.P., 2015. Peatland initiation and carbon dynamics in northeast China: links to Holocene climate variability. *BOREAS* 372, 575–587.
- Xu, D.K., Lu, H.Y., Chu, G.Q., Liu, L., Shen, C.M., Li, F.J., Wang, C., Wu, N.Q., 2019. Synchronous 500-year oscillations of monsoon climate and human activity in northeast Asia. *Nat. Commun.* 10 (1), 1–10.
- Xu, J., Morris, P.J., Liu, J., Holden, J., 2018. PEATMAP: refining estimates of global peatland distribution based on a meta-analysis. *Catena* 160, 134–140.
- Yang, Q.N., Liu, Z.P., Bai, E., 2023. Comparison of carbon and nitrogen accumulation rate between bog and fen phases in a pristine peatland with the fen–bog transition. *Glob. Change Biol.* 29, 6350–6366.
- Yu, Z.C., Beilman, D.W., Frolking, S., MacDonald, G.M., Roulet, N.T., Camill, P., Charman, D.J., 2011. Peatlands and their role in the global carbon cycle. *Eos Trans. Am. Geophys. Union* 92, 97–98.
- Zhang, M.M., Bu, Z.J., Jiang, M., Wang, S.Z., Liu, S.S., Jin, Q., Shi, P.H., 2019. Mid-late Holocene maar lake-mire transition in northeast China triggered by hydroclimatic variability. *Quat. Sci. Rev.* 220, 215–229.
- Zhao, Y., Yu, Z.C., Tang, Y., Li, H., Yang, B., Li, F.R., Zhao, W.W., Sun, J.H., Chen, J.H., Li, Q., Zhou, A.F., 2014. Peatland initiation and carbon accumulation in China over the last 50,000 years. *Earth Sci. Rev.* 128 (128), 139–146.
- Zheng, Y.H., Pancost, R.D., Liu, X.D., Wang, Z., Naffs, B.D.A., Xie, X., Liu, Z., Yu, X., Yang, H., 2017. Atmospheric connections with the North Atlantic enhanced the deglacial warming in northeast China. *Geology* 45, 1031–1034.
- Zhong, Y.H., Jiang, M., Middleton, B.A., 2020. Effects of water level alteration on carbon cycling in peatlands. *Ecosys. Health Sustain.* 6 (1), 1806113.